Turk J Elec Engin, VOL.14, NO.2 2006, © TÜBİTAK

Adaptive 3D Visual Servo Control of Robot Manipulators via Composite Camera Inputs*

Türker ŞAHİN and Erkan ZERGEROĞLU
Department of Computer Engineering, Gebze Institute of Technology,
PK. 141, 41400 Gebze/Kocaeli-Turkey.
e-mail: {htsahin,ezerger}@bilmuh.gyte.edu.tr

Abstract

This paper considers the problem of position control of robot manipulators via visual servoing in the presence of uncertainty associated with the robot dynamics and the vision system. Specifically, an adaptive controller is designed to compensate for the uncertainties associated with the mechanical parameters of the robot manipulator and the intrinsic parameters of the cameras. The 3D visual information is obtained from the composite inputs of two separate cameras placed in the robot work space. Despite the uncertainties associated with the camera system and robot dynamics the proposed adaptive controller achieves asymptotic end effector position tracking. A Lyapunov based approach is presented to prove the stability and boundedness of the signals in the closed loop system. Simulation results are presented to illustrate the performance of the proposed controller.

1. Introduction

Sensor based control is imperative for efficient control and operation of robotic manipulators. In most robot control systems, feedforward and feedback terms in the control algorithm are computed via the use of position and velocity information obtained by sensors located at each robot link (*e.g.*, encoders, resolvers, tachometers, *etc.*). However, when the robot is operating in an unstructured environment, such sensor information is not always satisfactory. In unstructured environments vision based systems allowing non-contact measurement of the surroundings, similar to human sense of sight, can be utilized for obtaining the position information required by the controller. Taken to the extreme, the visual sensor data can be applied for on-line trajectory planning and even for the feedforward/feedback control referred as visual servoing. An overview of the state-of-the-art in robot visual servoing can be found in [1, 2, 3]. In this work we will concentrate on a sub-class of visual servoing systems, referred as "*direct visual servoing*" where the visual data is used to compute the input to the dynamic model (actuator torques or forces) of the manipulator, as opposed to the *indirect visual servoing* where the output of the system is a control reference law that is then, fed into a low-level controller of the dynamical system model [1, 3].

Vision systems, used for robotic applications are mostly classified as a function of the number of vision sensors they use. That is: *i)* monocular visual servoing that uses one camera, either attached to a fixed place

*This work is supported by the Turkish State Planning Organization Grant DPT-2003K120530.

pointing towards the robotic work-space (fixed camera configuration) or mounted at the end effector of the robot (eye-in-hand configuration). *ii)* multi camera vision systems where, as the name indicates, multiple cameras placed in the work-space are used to collect the task specific information. While the monocular visual servoing offers a cheaper solution, as the cost of hardware and the associated software development process is highly reduced compared to multiple camera visual servoing, nearly in all applications the depth information of the work-space is lost. On the other hand even by the use of multiple cameras it is not always possible to extract all of the 6-DOF information (position and orientation of the end effector). Another drawback of using a camera system is to relate the image space measurements to the actual task-space variables also known as the camera calibration problem. Due to the presence of uncertainties in the camera calibration parameters, it is usually difficult to obtain intrinsic camera parameters (i.e. the image center , magnification factors, and camera scaling factor), and the extrinsic camera parameters (position and orientation of the camera within the work-space) exactly. Motivated by these, researchers presented quite a lot of solutions to camera calibration problem, unfortunately most solutions did not take the robot dynamics into account [4, 5, 6] thus are limited to the kinematic level. To achieve high performance it is imperative for a controller to incorporate the system dynamics into the control loop. This fact motivated the researchers to corporate the manipulator dynamics in to the control system design. For the monocular case, adaptive and robust controllers have been proposed [7, 8, 9]. Especially in [8] and [9], the proposed adaptive and robust controllers can compensate for the uncertainties associated with the camera system (intrinsic and extrinsic) and the dynamics of the manipulator. Unfortunately the monocular visual servoing constrains the problem to the 2D case and ignores depth information by concentrating on the planar robot manipulators where the out of plane motion is not possible. Recently, the focus in visual servoing has shifted towards 3D problems [3, 10, 11]. In [10], an asymptotically stable position based visual feedback controller has been presented, which can compensate the uncertainties of the homogeneous transformation matrix between the task-space and the camera space; however the controller assumes that the intrinsic camera parameters are perfectly calibrated. Another solution is [11], which is a PI-controller based 3D pose servoing scheme. This system gives accurate position and orientation control for stationary target applications , but was unable to avoid noticeable error fluctuations for tracking problems.

The visual system designed in this paper[1] belongs to the class of multi-camera visual servoing systems. Specifically, the result given in [8] have been extended to 3D position servoing case via the use outputs from 2 cameras. The outputs of the cameras are composed to represent the 3D Cartesian space information in the camera space. Then the composite camera calibration matrix is premultiplied by a transformation matrix, (similar to [8]) so that the resultant matrix is positive-definite and symmetric, which enabled us to incorporate the camera parameters into the robot equation using a backstepping technique [13]. The proposed visual control system only requires the knowledge of position of the cameras with respect to the base of the robotics manipulator and achieves asymptotic end effector position tracking despite the uncertainties in the camera calibration parameters and the robot dynamics.

The rest of the paper is organized as follows. In Section 2 the manipulator and the camera model used are presented. In Section 3 the control objective, controller development and stability analysis is presented, while the simulation results are presented in Section 4. Concluding remarks are summarized in Section 5.

[1] A preliminary version of this work has appeared at [12]

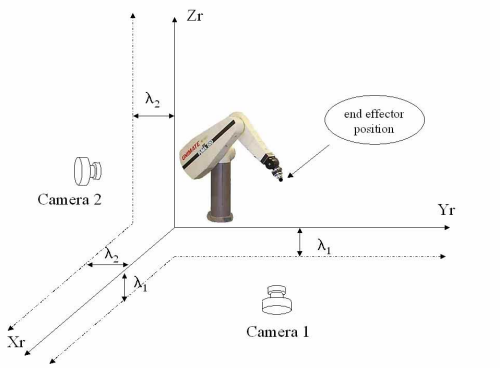

Figure 1. Placement of the Camera System with respect to Robot Coordinates

2. Robot-Camera Model

A schematic representation of the robot-camera system configuration considered in this work is given in Figure 1. We assume that the cameras are located at fixed points outside, but pointing towards the robot work-space such that: *i)* the image planes of camera 1 and camera 2 are parallel to $X_r - Y_r$ and $X_r - Z_r$ planes of motion of the robot respectively; and *ii)* both cameras can capture images throughout the entire robot work-space.

2.1. Robot Dynamics

The joint-space model for a three link, revolute, direct-drive, robot manipulator is assumed to be of the form [14]

$$M(q)\ddot{q} + V_m(q,\dot{q})\dot{q} + G(q) + F(\dot{q}) = \tau, \tag{1}$$

where $q(t)$, $\dot{q}(t)$, $\ddot{q}(t) \in \mathbb{R}^3$ denote the link position, velocity and acceleration vectors, respectively; $M(q) \in \mathbb{R}^{3\times3}$ represents the link inertia matrix, $V_m(q,\dot{q}) \in \mathbb{R}^{3\times3}$ represents centripetal-Coriolis matrix, $G(q) \in \mathbb{R}^3$ represents the gravity effects, $F(\dot{q}) \in \mathbb{R}^3$ represents the friction effects, and $\tau(t) \in \mathbb{R}^3$ represents the torque input vector.

The robot dynamics given in (1) have the following useful properties [15]:

Property 1: The inertia matrix $M(q)$ is symmetric and positive-definite, and satisfies the inequalities

$$m_1 \|\xi\|^2 \leq \xi^T M(q)\xi \leq m_2 \|\xi\|^2 \ \ \forall \xi \in \mathbb{R}^3, \tag{2}$$

where $m_1, m_2 \in \mathbb{R}$ are positive bounding constants, and $\|\cdot\|$ denotes the standard Euclidean norm.

Property 2: The inertia and centripetal-Coriolis matrices satisfy the following skew symmetric relationship

$$\xi^T \left(\frac{1}{2}\dot{M}(q) - V_m(q,\dot{q}) \right) \xi = 0 \qquad \forall \xi \in \mathbb{R}^3, \tag{3}$$

where $\dot{M}(q)$ denotes the time derivative of the inertia matrix.

Property 3: The dynamic model in (1) can be linearly parameterized (as shown below) as

$$M(q)\ddot{q} + V_m(q,\dot{q})\dot{q} \ + G(q) + F(\dot{q}) = W\left(q,\dot{q},\ddot{q}\right)\varphi, \tag{4}$$

where $\varphi \in \mathbb{R}^m$ contains the constant system parameters, and the regression matrix $W(\cdot) \in \mathbb{R}^{3\times m}$ contains known functions dependent on the signals $q(t)$, $\dot{q}(t)$, and $\ddot{q}(t)$ (it is assumed that if the arguments of $W(\cdot)$ are bounded then $W(\cdot)$ is bounded).

Remark 1 *For simplicity, the above model has been developed for a non-redundant robot manipulator (i.e., we assume $n = 3$); and the formulation is based on only end effector position tracking problem. However, the results delineated in this paper, with minor modifications, can be extended to the redundant case (see [8] for details) and might serve as a stepping stone for the full order, end effector position plus orientation tracking in cartesian space (see [16] for details).*

2.2. Composite Camera Model Development

Using the standard pin-hole model for a camera system, a point $X_r = \left[\begin{array}{ccc} x_r & y_r & z_r \end{array}\right]^T$ in a 3-D world frame can be represented in terms of camera space coordinate frame as [17]

$$\left[\begin{array}{c} x_c \\ y_c \end{array}\right] = \frac{f}{z_r}\left[\begin{array}{cc} \beta_1 & 0 \\ 0 & \beta_2 \end{array}\right] R(\theta)\left\{\left[\begin{array}{c} x_r \\ y_r \end{array}\right] - \left[\begin{array}{c} o_1 \\ o_2 \end{array}\right]\right\} + \left[\begin{array}{c} c_1 \\ c_2 \end{array}\right], \tag{5}$$

where $Y = \left[\begin{array}{cc} x_c & y_c \end{array}\right]^T$ denotes the corresponding position vector in camera space, f is the focal length of the lens used, β_1, β_2 are the magnification factors of the camera, $R(\theta) \in \mathbb{R}^{2\times 2}$ is the rotation matrix defined as

$$R(\theta) = \left[\begin{array}{cc} \cos\theta & -\sin\theta \\ \sin\theta & \cos\theta \end{array}\right] \tag{6}$$

with θ being the rotation angle of the camera, $O = \left[\begin{array}{cc} o_1 & o_2 \end{array}\right]^T$ is the position of the optical center of the camera with respect to the world coordinate frame and $C = \left[\begin{array}{cc} c_1 & c_2 \end{array}\right]^T$ denotes the image center which is defined as the frame buffer coordinates of the intersection of the optical axis with the image plane. Using the camera transformation given in (5) the camera space variables of camera 1 in the system shown in Figure 1 are obtained as

$$\left[\begin{array}{c} x_{c1} \\ y_{c1} \end{array}\right] = \frac{1}{z_r + \lambda_1} H_1 R(\theta_1)\left[\begin{array}{c} x_r - o_{11} \\ y_r - o_{12} \end{array}\right] + \left[\begin{array}{c} p_{11} \\ p_{12} \end{array}\right], \tag{7}$$

where $H_1 \in \mathbb{R}^{2\times 2}$ is defined as

$$H_1 = \left[\begin{array}{cc} f_1\beta_{11} & 0 \\ 0 & f_1\beta_{12} \end{array}\right]. \tag{8}$$

Similarly, camera 2 variables are

$$\left[\begin{array}{c} x_{c2} \\ z_{c2} \end{array}\right] = \frac{1}{y_r + \lambda_2} H_2 R(\theta_2)\left[\begin{array}{c} x_r - o_{21} \\ z_r - o_{22} \end{array}\right] + \left[\begin{array}{c} p_{21} \\ p_{22} \end{array}\right], \tag{9}$$

where $H_1, H_2, R(\theta_1), R(\theta_2) \in \mathbb{R}^{2\times 2}$ and $p_1 = \left[\begin{array}{cc} p_{11} & p_{12} \end{array}\right]^T, p_{21} = \left[\begin{array}{cc} p_{21} & p_{22} \end{array}\right]^T \in \mathbb{R}^{2\times 1}$ are constant but unknown camera parameters, and $\lambda_1, \lambda_2,\ o_{11},\ o_{12},\ o_{21},\ o_{22}$ are positive constants representing the placement of the camera with respect to the origin of the robot world coordinate frame and are assumed to be known. Our first goal is to obtain a composite camera input from the two camera inputs placed in the work space that can lead us to obtain 3 dimensional position information (x_r, y_r, z_r) about the object in the work space as opposed to the normal 2-D projection using a standard camera. To this extent, using the properties of the rotation matrix and the fact that H_2 is a diagonal matrix, z_{c2} defined in (9) can be written in the form

$$z_{c2} = \gamma_1 \frac{z_r - o_{22}}{y_r + \lambda_2} + \gamma_2 x_{c2} + \gamma_3, \tag{10}$$

where the constant parameters $\gamma_1,\ \gamma_2,\ \gamma_3 \in \mathbb{R}$ are explicitly defined as

$$\gamma_1 \ = \ \frac{f_2 \beta_{22}}{\cos\theta_2},\ \gamma_2 = \frac{\beta_{22}\sin\theta_2}{\beta_{21}\cos\theta_2},\ \text{and}\ \ \gamma_3 = p_{22} - p_{21}\frac{\beta_{22}\sin\theta_2}{\beta_{21}\cos\theta_2}. \tag{11}$$

Based on (7) and (11), we find the composite camera input representation as

$$\left[\begin{array}{c} x_{c1} \\ y_{c1} \\ z_{c2} \end{array}\right] = \overbrace{\left[\begin{array}{cc} H_1 R(\theta_1) & 0_{2\times 1} \\ 0_{1\times 2} & \gamma_1 \end{array}\right]}^{\triangleq H\cdot R} \left[\begin{array}{c} \frac{x_r - o_{11}}{z_r + \lambda_1} \\ \frac{y_r - o_{12}}{z_r + \lambda_1} \\ \frac{z_r - o_{22}}{y_r + \lambda_2} \end{array}\right] + \left[\begin{array}{c} p_{11} \\ p_{12} \\ \gamma_2 x_{c2} + \gamma_3 \end{array}\right]. \tag{12}$$

For simplicity, we defined the composite camera input vector $X_c = \left[\begin{array}{ccc} x_{c1} & y_{c1} & z_{c2} \end{array}\right]^T$ and the off-setted cartesian vector $X_{\overline{R}} \in \mathbb{R}^3$ as

$$X_{\overline{R}} \triangleq \left[\begin{array}{c} \overline{x_r} \\ \overline{y_r} \\ \overline{z_r} \end{array}\right] = \left[\begin{array}{c} x_r - o_{11} \\ y_r - o_{12} \\ z_r - o_{22} \end{array}\right]. \tag{13}$$

Note that $X_{\overline{R}}$ can be calculated using the forward kinematics of the robot and the camera positioning values $o_{11}, o_{12},\ o_{22}$. Taking the time derivative of (12), we obtain the following differential relationship between X_c and $X_{\overline{R}}$:

$$\dot{X}_c = HRJ_c\dot{X}_{\overline{R}} + \left[\begin{array}{c} 0 \\ 0 \\ \gamma_2 \dot{x}_{c2} \end{array}\right], \tag{14}$$

where the composite camera image Jacobian, $J_c \in \mathbb{R}^{3\times 3}$ is defined explicitly as

$$J_c = \left[\begin{array}{ccc} \frac{1}{(\overline{z_r}+\lambda_1+o_{22})} & 0 & -\frac{\overline{x_r}}{(\overline{z_r}+\lambda_1+o_{22})^2} \\ 0 & \frac{1}{(\overline{z_r}+\lambda_1+o_{22})} & -\frac{\overline{y_r}}{(\overline{z_r}+\lambda_1+o_{22})^2} \\ 0 & -\frac{\overline{z_r}}{(\overline{y_r}+\lambda_2+o_{12})^2} & \frac{1}{(\overline{y_r}+\lambda_2+o_{12})} \end{array}\right]. \tag{15}$$

For our analysis to hold, the composite image Jacobian matrix J_c has to be invertible (in other words, $\det(J_c)$ have to be non-zero). For this reason the denominators of the entries in equation (15) have to be non-zero. Accordingly $\lambda_2 + o_{12}$, and $\lambda_1 + o_{22}$ are both selected to be positive and the motion of the manipulator is restricted to one quadrant to provide also positive values for $\overline{y_r}$, and $\overline{z_r}$.

3. Control Formulation and Design

We will assume that a smooth, time varying, desired end effector trajectory generated in the camera space, denoted by $X_d(t) = \left[\begin{array}{ccc} x_d(t) & y_d(t) & z_d(t) \end{array} \right]^T$ is constructed so that $X_d(t) \in C^2$. To provide a means of quantifying the position tracking control objective, we defined the position tracking error signal in camera space $e(t) \in \mathbb{R}^3$ as

$$e = X_d - X_c. \tag{16}$$

Taking time derivative of (16) and multiplying the resultant equation by

$$A \triangleq \left[\begin{array}{ccc} A_1 & A_2 & 0 \\ A_3 & A_4 & 0 \\ 0 & 0 & A_5 \end{array} \right] = (H\,R)^{-1} = \left[\begin{array}{ccc} \frac{\cos\theta_1}{f_1\beta_{11}} & \frac{\sin\theta_1}{f_1\beta_{12}} & 0 \\ -\frac{\sin\theta_1}{f_1\beta_{11}} & \frac{\cos\theta_1}{f_1\beta_{12}} & 0 \\ 0 & 0 & \frac{1}{\gamma_1} \end{array} \right], \tag{17}$$

we obtain

$$A\dot{e} = A\left\{ \dot{X}_d - \left[\begin{array}{c} 0 \\ 0 \\ \gamma_2 \dot{x}_{c2} \end{array} \right] \right\} - J_c\, J\, \dot{q}. \tag{18}$$

Note that the forward kinematic relationship $\dot{X}_{\overline{R}} = J\dot{q}$ is utilized. Motivated by the subsequent stability analysis, we pre-multiply both sides of (18) by the transformation matrix

$$T = \left[\begin{array}{ccc} \frac{1}{A_1A_4 - A_3A_2} & \frac{A_3}{A_4} - \frac{A_2}{A_4(A_1A_4 - A_3A_2)} & 0 \\ 0 & 1 & 0 \\ 0 & 0 & 1 \end{array} \right] \tag{19}$$

and obtain the open loop dynamics for $\dot{e}(t)$ as

$$Z\dot{e} = Z\left\{ \dot{X}_d - \left[\begin{array}{c} 0 \\ 0 \\ \gamma_2 \dot{x}_{c2} \end{array} \right] \right\} - T J_c\, J\, \dot{q}, \tag{20}$$

where the constant matrix $Z \in \mathbb{R}^{3\times 3}$ is defined in the form

$$Z = \left[\begin{array}{ccc} \frac{1+A_3^2}{A_4} & A_3 & 0 \\ A_3 & A_4 & 0 \\ 0 & 0 & A_5 \end{array} \right]. \tag{21}$$

Notice that $Z \in \mathbb{R}^{3\times 3}$ is positive definite and symmetric, when the rotation angles of the cameras satisfy $-\pi/2 < \theta_1, \theta_2 < \pi/2$. Following a backstepping-like design procedure [13], we can rewrite (20) to have the form

$$Z\dot{e} = Z\left\{ \dot{X}_d - \left[\begin{array}{c} 0 \\ 0 \\ \gamma_2 \dot{x}_{c2} \end{array} \right] \right\} - Tv + T J_I\, \eta. \tag{22}$$

In (22) the term $J_I \triangleq J_c\, J$ is the image Jacobian and the auxiliary tracking-like signal $\eta(t) \in \mathbb{R}^3$ is defined as

$$\eta = u - \dot{q} \tag{23}$$

with $u = J_I^{-1} v$. Using the definitions of (19) and (21) the open loop dynamics of (22) can be written in the following advantageous form:

$$Z\dot{e} = \begin{bmatrix} \phi_4^{-1}(W_1\phi_1 - v_1) \\ W_2\phi_2 - v_2 \\ W_3\phi_3 - v_3 \end{bmatrix} + TJ_I\,\eta, \tag{24}$$

where $W_1(.)$, $W_2(.)$, $W_3(.)$ are known regression matrices defined explicitly as

$$W_1 = \begin{bmatrix} \dot{x}_d & \dot{y}_d & -v_2 \end{bmatrix},\ W_2 = \begin{bmatrix} \dot{x}_d & \dot{y}_d \end{bmatrix},\ W_3 = \begin{bmatrix} \dot{z}_d & \dot{x}_{c2} \end{bmatrix}, \tag{25}$$

and ϕ_1, ϕ_2, ϕ_3, ϕ_4 represents unknown constant parameter vectors with proper dimensions that are defined as

$$\begin{aligned} &\phi_1 = \begin{bmatrix} \frac{1+A_3^2}{A_4}\phi_4 & A_3\phi_4 & \frac{A_3\phi_4 - A_2}{A_4} \end{bmatrix}^T,\ \ \phi_2 = \begin{bmatrix} A_3 & A_4 \end{bmatrix}^T, \\ &\phi_3 = \begin{bmatrix} \frac{1}{\gamma_1} & -\frac{\gamma_2}{\gamma_1} \end{bmatrix}^T,\ \ \phi_4 = A_1A_4 - A_2A_3. \end{aligned} \tag{26}$$

Based on the open-loop dynamics and the subsequent stability analysis the auxiliary internal control inputs are designed as

$$\begin{aligned} v_1 &= W_1\hat{\phi}_1 + k_1e_1,\ v_2 = W_2\hat{\phi}_2 + k_2e_2, \\ \text{and } v_3 &= W_3\hat{\phi}_3 + k_3e_3, \end{aligned} \tag{27}$$

where $e_i(t)$, $i = 1,2,3$ denote the elements of $e(t)$, k_1, k_2, k_3 are positive, scalar control gains and $\hat{\phi}_1(t) \in \mathbb{R}^3$, $\hat{\phi}_2(t) \in \mathbb{R}^2$, $\hat{\phi}_3(t) \in \mathbb{R}^2$are dynamic parameter estimates that are updated according to

$$\dot{\hat{\phi}}_1 = \Gamma_1 W_1^T e_1,\ \dot{\hat{\phi}}_2 = \Gamma_2 W_2^T e_2\,,\ \dot{\hat{\phi}}_3 = \Gamma_3 W_3^T e_3, \tag{28}$$

where $\Gamma_1 \in \mathbb{R}^{3\times3}$, $\Gamma_2 \in \mathbb{R}^{2\times2}$and $\Gamma_3 \in \mathbb{R}^{2\times2}$ are diagonal, positive-definite, gain matrices. After substituting (27) into (24) we obtain the closed loop dynamics for $e(t)$ as

$$Z\dot{e} = \begin{bmatrix} \phi_4^{-1}(W_1\tilde{\phi}_1 - k_1e_1) \\ W_2\tilde{\phi}_2 - k_2e_2 \\ W_3\tilde{\phi}_3 - k_3e_3 \end{bmatrix} + TJ_I\,\eta. \tag{29}$$

The backstepping type control design also requires the dynamics for the auxiliary signal $\eta(t)$; to obtain this, we take the time derivative of (23) and pre-multiply the resultant equation by the inertia matrix to obtain

$$M\dot{\eta} = -V_m\eta - J_I^T T^T e - \tau + Y\theta, \tag{30}$$

where $Y(.)$ is a regression matrix containing the known/measurable terms and θ is the vector containing unknown but constant system parameters with proper dimensions such that $Y\theta$ is expressed as

$$Y\theta = M\dot{u} + V_m u + F(\dot{q}) + G + J_I^T T^T e \tag{31}$$

Note that the term $J_I^T T^T e$ is injected to the dynamics to cancel the corresponding term in stability analysis.

Remark 2 *Based on the structure of (31) and standard adaptive controller design procedures, it is fairly easy to see that when the control torque input vector* $\tau(t)$ *with the parameter estimation vector* $\hat{\theta}(t)$ *is designed to have the form*

$$\begin{aligned} \tau &= Y\hat{\theta} + K_\eta \eta \\ \dot{\hat{\theta}} &= \Gamma_\theta Y^T \eta, \end{aligned} \tag{32}$$

where $K_\eta \in R^{n\times n}$ *is a constant, diagonal, positive definite, gain matrix and* Γ_θ *is a constant, diagonal, positive definite matrix with proper dimension, the tracking error can be driven to zero. However, as can be observed from (31) and (32), this approach requires the calculation of the time derivative of the auxiliary control input* $u(t)$, *which in turns necessitates the calculations of the derivatives of the input* $v(t)$ *and the image Jacobian* J_I *on line. Thus, the implementation would require massive computations and hinders the analysis making the result unnecessarily complicated for practical purposes. In this work, instead of using the aforementioned standard adaptive controller approach, we will utilize a high gain controller that would treat the regression matrix multiplied by the uncertain parameter vector formulation as if it were a disturbance term and utilize a nonlinear damping argument to compensate for the unwanted effects of it. This method not only eases the implementation but also preserves the asymptotic stability result, as will be presented in the subsequent analysis.*

Utilizing the fact that the system dynamics $Y\theta$ is bounded by a function of the form

$$\|Y\theta\| \leq \rho(\|x\|)\,\|x\|\,, \tag{33}$$

with $x = \begin{bmatrix} e^T & \eta^T \end{bmatrix}$, the control torque input vector is designed to be

$$\tau = k_n \rho(\|x\|)^2 \eta + K_\eta \eta, \tag{34}$$

where $K_\eta \in \mathbb{R}^{n\times n}$ is a constant, diagonal, positive definite, gain matrix. After substituting (34) in (30) with the dynamics bounded according to equation (33), we obtain the closed loop dynamics for $\eta(t)$ as

$$M\dot{\eta} = -V_m\eta - J_I^T T^T e - K_\eta \eta - k_n \rho(\|x\|)^2 \eta + Y\theta. \tag{35}$$

We now state the following Theorem.

Theorem 1 *The adaptive control law proposed by (27) with the update laws (28) and the control law of (34) ensure the global asymptotic end effector tracking in the sense that*

$$\lim_{t\to\infty} e(t) = 0, \tag{36}$$

provided that the damping gain obeys the inequality

$$k_n \geq \frac{1}{4\min(\lambda_{\min}\{K_\eta\}, \min(\phi_4^{-1}k_1, k_2, k_3))} \tag{37}$$

and the camera orientations satisfy the condition

$$-\pi/2 < \theta_i < \pi/2, \quad i = 1, 2\,. \tag{38}$$

Proof 1 *We begin our proof by introducing the following non-negative scalar function:*

$$V = \frac{1}{2}e^T Ze + \frac{1}{2}\eta^T M\eta + \frac{1}{2}\phi_4^{-1}\tilde{\phi}_1^T\Gamma_1^{-1}\tilde{\phi}_1 + \frac{1}{2}\tilde{\phi}_2^T\Gamma_2^{-1}\tilde{\phi}_2 + \frac{1}{2}\tilde{\phi}_3^T\Gamma_3^{-1}\tilde{\phi}_3. \tag{39}$$

Taking the time derivative of this expression, then inserting the closed loop dynamics from (29) and (35), and applying the parameter update terms in (28), we obtain the relationship

$$\begin{aligned}\dot{V} &= e_1\phi_4^{-1}W_1\tilde{\phi}_1 - k_1e_1^2 + e_2W_2\tilde{\phi}_2 - k_2e_2^2 + e_3W_3\tilde{\phi}_3 - k_3e_3^2 + e^TTJ_I\eta \\ &\quad + \frac{1}{2}\eta^T\dot{M}\eta + \eta^T(-V_m\eta - J_I^TT^Te - K_\eta\eta - k_n\rho(\|x\|)^2\eta + Y\theta) \\ &\quad - \phi_4^{-1}\tilde{\phi}_1^TW_1^Te_1 - \tilde{\phi}_2^TW_2^Te_2 - \tilde{\phi}_3^TW_3^Te_3,\end{aligned} \tag{40}$$

to which when we apply the skew symmetric relationship between the inertia and centripetal-Coriolis matrices in (3) and eliminate the corresponding parameter error and image Jacobian J_I terms, followed by substitution of (33) for the system dynamics, we obtain:

$$\begin{aligned}\dot{V} &\leq -\phi_4^{-1}k_1e_1^2 - k_2e_2^2 - k_3e_3^2 - \eta^TK_\eta\eta \\ &\quad -[\eta^Tk_n\rho(\|x\|)^2\eta) - \eta^T\rho(\|x\|)\,\|x\|].\end{aligned} \tag{41}$$

By adding and subtracting $\frac{\|x\|^2}{4k_n}$ terms to the right hand side of this equation, we can complete the squares of the nonlinear damping gain and the system dynamics bounding functions in the second line of (41), thus can further upperbound this result to have the following form:

$$\begin{aligned}\dot{V} &\leq -\phi_4^{-1}k_1e_1^2 - k_2e_2^2 - k_3e_3^2 - \eta^TK_\eta\eta \\ &\quad - \left[\sqrt{k_n}\rho(\|x\|)\,\|\eta\| - \frac{\|x\|}{2\sqrt{k_n}}\right]^2 + \frac{\|x\|^2}{4k_n}.\end{aligned} \tag{42}$$

As the completed squares term in (42) has a negative value for all times, its presence has no effect on the validity of this inequality, hence the rest of the term in (42) can be expressed to have the form

$$\dot{V} \leq -\beta\,\|x\|^2, \tag{43}$$

where $\beta = \min\left\{\lambda_{\min}\{K_\eta\},\ \min(\phi_4^{-1}k_1, k_2, k_3)\right\} - \frac{1}{4k_n}$ and the definition (33) has been applied for x. From (39) and (43), provided that (37) is satisfied, we can conclude that $V(t) \in \mathcal{L}_\infty$; hence, all the elements of $V(t)$, that is $e(t)$, $\eta(t)$, $\tilde{\phi}_1(t)$, $\tilde{\phi}_2(t)$, and $\tilde{\phi}_3(t) \in \mathcal{L}_\infty$. Furthermore, using the boundedness of the tracking error signal $e(t)$ and the estimation error terms $\tilde{\phi}_i(t),\ i = 1,2,3$, the auxiliary control terms $v_i(t),\ i = 1,2,3$ from (27) are also bounded. Due to the boundedness of $\eta(t)$ and $\rho(\|x\|)$, from equation (34), the control torque input $\tau(t)$ is also bounded. Similarly from (28), the boundedness of $\dot{\hat{\phi}}_i(t),\ i = 1,2,3$ are achieved. So we have proven that all the signals remain bounded during the closed loop operation. At this stage, using the boundedness of $v_i(t)$ and $\eta(t)$ terms in equation (29) of closed loop error dynamics, we can also show that $\dot{e}(t)$ is bounded. Due to the boundedness of $\dot{e}(t)$, we can conclude that $e(t)$ is uniformly continuous. In addition, it is straightforward to use (43) to illustrate that $e(t) \in \mathcal{L}_2$. At this point from direct application of Barbalat's Lemma [18] we conclude (36) $\square$.

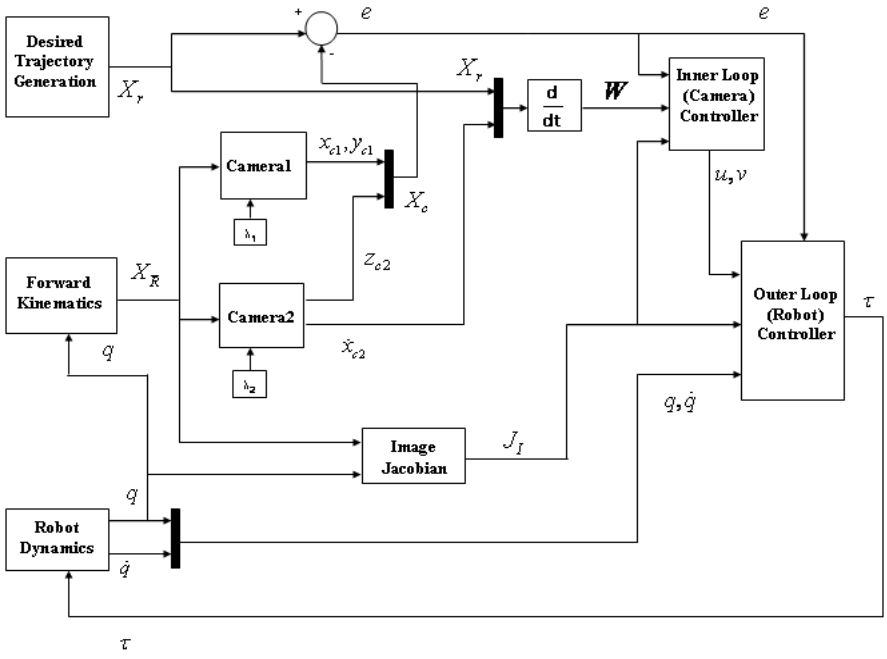

Figure 2. The block diagram of the designed visual servo system

4. Simulation Results

A block diagram of the applied visual servoing configuration is given in Figure 2. The functions of the main blocks in this figure can be summarized as follows. The actual robot trajectories, $X_{\bar{R}}$, from the robot forward kinematics block are observed by cameras 1 and 2 to form the 3-D composite camera output, $X_c(t)$. This camera output is compared with the desired trajectory, $X_r(t)$, the difference of which is fed to the camera controller as the error signal $e(t)$. The output from the camera controller, namely the auxiliary signals, u and v are applied with the Image Jacobian J_I to the robot controller. This controller updates the robot dynamics by applying the control torque signal τ, and the output of dynamics block is applied to the forward kinematics block for the cartesian space vector $X_{\bar{R}}$. This vector is again fed to the composite camera setup, and the system keeps functioning on in this manner.

The applied dynamical model is a 3-dof robot manipulator with the following inertia, centripetal-Coriolis and gravity matrices:

$$M = \begin{bmatrix} M_{11} & 0 & 0 \\ 0 & M_{22} & M_{23} \\ 0 & M_{32} & M_{33} \end{bmatrix}, \tag{44}$$

$$V_m = \begin{bmatrix} V_{11} & 0 & 0 \\ 0 & V_{22} & V_{23} \\ 0 & V_{32} & 0 \end{bmatrix}, \quad G = \begin{bmatrix} 0 \\ G_2 \\ G_3 \end{bmatrix}.$$

Here, the entries are formulated as

$$\begin{aligned} M_{11} = \; & m_3(l_2\cos(q_2)+l_{c3}\cos(q_2+q_3))^2 + m_2 l_{c2}^2\cos^2(q_2) \\ & + A_2\sin^2(q_2) + A_3\sin^2(q_2+q_3) + E_1 \\ & + E_3\cos^2(q_2) + E_3\cos^2(q_2+q_3) \end{aligned} \tag{45}$$

$$M_{22} = \; m_2 l_{c2}^2\sin^2(q_2) + l_2 + l_3 + m_3(l_2^2 + l_{c3}^2 + 2l_2 l_{c3}\cos(q_3))$$

$$M_{23} = \; M_{32} = m_3(l_{c3}^2 + l_2 l_{c3}\cos(q_3)) + l_3$$

$$M_{33} = \; m_3 l_{c3} + l_3$$

$$\begin{aligned} V_{11} = \; & -m_3 l_2 l_{c3}(\dot{q}_2+\dot{q}_3)\sin(q_2+q_3)\cos(q_2) \\ & - m_3 l_2 l_{c3}\dot{q}_2\sin(q_2)\cos(q_2+q_3) \\ & - (m_2 l_{c2}^2 + m_3 l_2^2 + E_3)\dot{q}_2\sin(q_2)\cos(q_2) \\ & - (m_3 l_{c3}^2 + E_3)(\dot{q}_2+\dot{q}_3)\sin(q_2+q_3)\cos(q_2+q_3) \\ & + A_2\dot{q}_2\sin(q_2)\cos(q_2) + A_3(\dot{q}_2+\dot{q}_3)\sin(q_2+q_3)\cos(q_2+q_3) \end{aligned} \tag{46}$$

$$V_{22} = \; -m_3 l_2 l_{c3}\dot{q}_3\sin(q_3) + m_2 l_{c2}^2\dot{q}_2\sin(q_2)\cos(q_2)$$

$$V_{23} = \; V_{32} = -0.5 m_3 l_2 l_{c3}\dot{q}_3\sin(q_3)$$

$$G_2 = \; 9.8(m_2 l_{c2} + m_3 l_2)\cos(q_2) + 9.8 m_3 l_{c3}\cos(q_2+q_3) \tag{47}$$

$$G_3 = \; 9.8 m_3 l_{c3}\cos(q_2+q_3).$$

In these matrices the applied coefficients are the lengths of the manipulator links $l_1 = 0.5$, $l_2 = 0.4$, $l_3 = 0.4$ in meters, the masses of the links $m_1 = 4, m_2 = 3$ and $m_2 = 3$ in kg, distances of the link joints $l_{c2} = 0.2$, $l_{c3} = 0.2$ in meters, and the cylindrical link radius $R = 0.05$. The torque limits are $\tau_i = \pm 50$ and the cylindrical link inertial parameters are obtained by $E_1 = m_1 R^2/2$, $E_i = m_i R^2/12$, $A_i = m_i R^2/2$ and $l_i = m_i R^2/12$, where $i = 2, 3$ for the robot links.

The controller parameters are tuned to the below values for the efficient operation of the designed visual servo system. Accordingly the internal (camera) controller gain matrix is

$$K \triangleq diag\{\; k_1 \quad k_2 \quad k_3 \;\} = diag\{\; 3 \quad 1.5 \quad 2 \;\} \tag{48}$$

and the applied adaptation term parameters are:

$$\begin{aligned} \Gamma_1 &= diag\{\; 0.5 \quad 0.0001 \quad 0.01 \;\} \\ \Gamma_2 &= diag\{\; 0.001 \quad 0.005 \;\} \\ \Gamma_3 &= diag\{\; 0.00005 \quad 0.00001 \;\}. \end{aligned} \tag{49}$$

Similarly, the outer loop (robot) control has the control gain matrix and the damping gain coefficient selected as

$$K_\eta = diag\{\; 50 \quad 75 \quad 25 \;\}, \quad k_n = 25. \tag{50}$$

For simulation results a sample desired position trajectory in the composite camera space is selected as

$$X_d(t) = \begin{bmatrix} 465 + 20\sin(\frac{\pi}{6}t + \frac{\pi}{12}) \\ 490 + 25\sin(\frac{\pi}{6}t + \frac{5\pi}{12}) \\ 480 + 20\sin(\frac{\pi}{6}t + \frac{5\pi}{12}) \end{bmatrix}, \tag{51}$$

with all components in pixels. Trajectories in similar ranges should be preferred as these do not force the singularities of the employed manipulator model.

The composite camera output for this trajectory is in Figure 3, from which the initial system transients can be observed to decay quickly. Similarly, the Figure 4 depicts the quick convergence of the error terms to zero, verifying the asymptotically stable nature of the proposed system. The applied controller torque outputs are in Figure 5, while Figure 6 shows the parameter estimates for the inner loop, which also converge in short time periods. As an overall result, these figures depict the stable and efficient operation of the presented visual servo configuration and hence should verify the validity of the controller system developed in this paper.

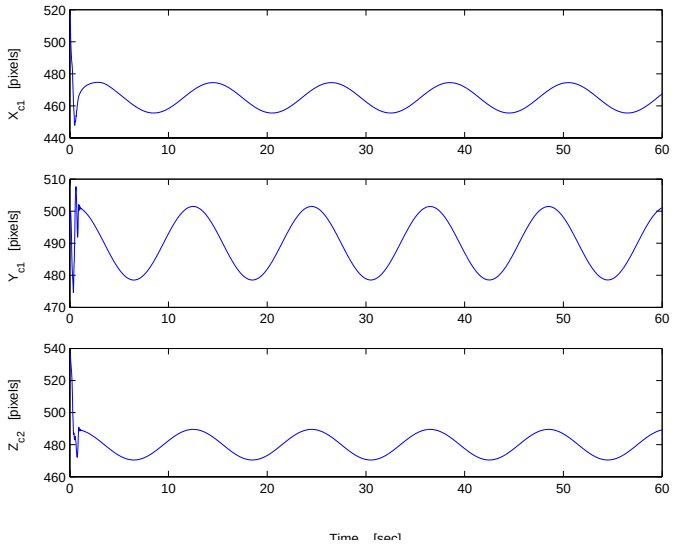

Figure 3. The End Effector Trajectory as seen from the Composite Camera during simulation.

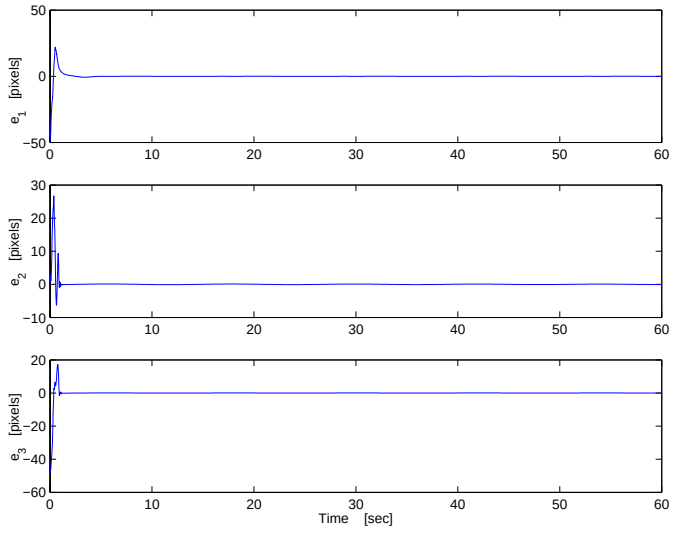

Figure 4. The Tracking Error Terms.

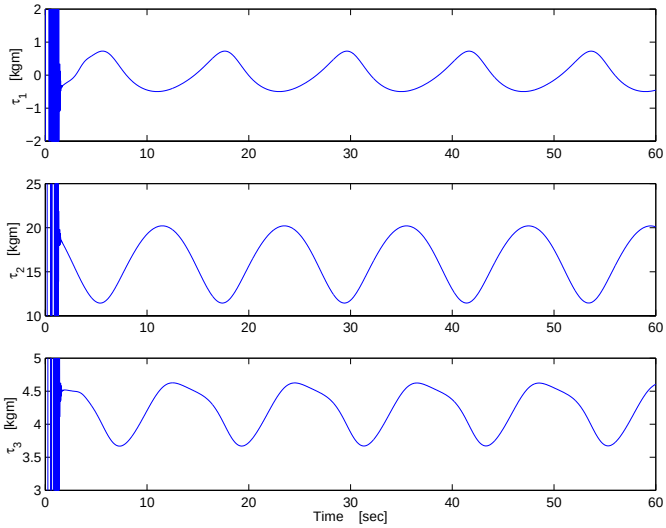

Figure 5. Input Control Torques.

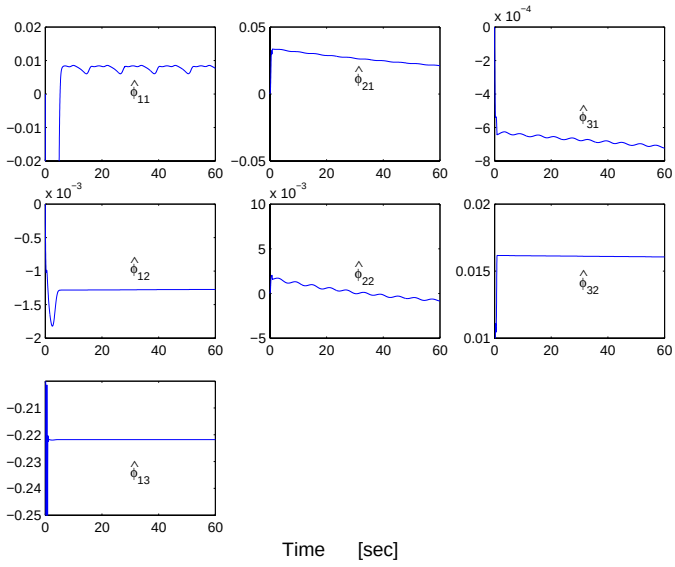

Figure 6. Estimates for the Uncertain Parameters of the Cameras.

5. Conclusion

We have presented a nonlinear, adaptive, 3-D end effector position tracking controller for a vision based system composed of 2 fixed cameras. The proposed controller achieves asymptotic end effector tracking despite the presence of uncertainties in some of the intrinsic camera parameters of both vision sensors and the robot dynamics. This result was obtained by applying a novel approach to compose the camera inputs to form the 3 dimensional end effector position information in camera space and using a backstepping design scheme. Considering the similarities between the controller design procedures our controller might be considered as the 3-D extension of [8] with the use of multiple cameras.

References

[1] G.D. Hager and S. Hutchinson (guest editors), Special Section on Vision-Based Control of Robot Manipulators, *IEEE Trans. Robotics and Automation*, Vol. 12, No. 5, Oct. 1996.

[2] B. Nelson and N. Papanikolopoulos (guest editors), Special Issue on Visual Servoing, *IEEE Robotics and Automation Mag.*, Vol. 5, No. 4, Dec. 1998.

[3] E. Malis, "Survey of Vision Based Control", *ENSIETA European Naval Ship Design Short Course*, Brest, France, 2002.

[4] F. Miyazaki and Y. Masutani, "Robustness of Sensory Feedback Control Based on Imperfect Jacobian", *Robotics Research: The Fifth Int. Symp.*, pp. 201-208, H. Miura and S. Arimoto, Eds., Cambridge, MA: MIT Press, 1990.

[5] G.D. Hager, W.C. Chang, and A.S. Morse, "Robot Hand-Eye Coordination Based on Stereo Vision", *IEEE Control Systems Mag.*, Vol. 15, No. 1, pp. 30-39, Feb. 1995.

[6] B. H. Yoshima and P. K. Allen, "Active, uncalibrated Visual Servoing", *in Proc. IEEE Int. Conf. Robotics and Automation*, pp 156-161, 1994.

[7] R. Kelly, "Robust Asymptotically Stable Visual Servoing of Planar Robots", *IEEE Trans. Robotics and Automation,* Vol 12, No. 5, pp.759-766, 1996.

[8] E. Zergeroglu, D. Dawson, M.S. de Queiroz, and A. Behal, "Vision-Based Nonlinear Tracking Controllers with Uncertain Robot-Camera Parameters ", *IEEE/ASME Transactions on Mechatronics,* Vol. 6, No 3, pp 322-337, September 2001.

[9] E. Zergeroglu, D. M. Dawson, M. S. de Queiroz, and P. Setlur, "Robust Visual-Servo Control of Planar Robot Manipulators in the presence of uncertainty", *Journal of Robotic Systems*, Volume 20, Issue 2, pp. 93-106, Feb. 2003.

[10] Y. Shen, D. Sun, Y. Lui, K. Li, "Asymptotic Trajectory Tracking of Manipulators Using Uncalibrated Visual Feedback", *IEEE/ASME Transactions on Mechatronics,* Vol. 8, No 1, pp 87-98, March 2003.

[11] M. Saedan and M. H. Ang Jr, "3D Vision-Based Control of an Industrial Robot", *Proceedings of the IASTED International Conference on Robotics and Applications,* Florida, USA, pp. 152-157, Nov. 19-22 2002.

[12] H.T. Şahin, E. Zergeroglu "Adaptive Visual Servo Control of Robot Manipulators via Composite Camera Inputs" *Fifth International Workshop on Robot Motion and Control-ROMOCO05*, pp. 219-224, Dymaczewo-Poland, June 2005

[13] M. Krstic, I. Kanellakopoulos, and P. Kokotovic, *Nonlinear and Adaptive Control Design*, New York, NY: John Wiley and Sons, 1995.

[14] M.W. Spong and M. Vidyasagar, *Robot Dynamics and Control*, New York, NY: John Wiley and Sons, 1989.

[15] F.L. Lewis, C.T. Abdallah, and D.M. Dawson, *Control of Robot Manipulators*, New York, NY: MacMillan, 1993.

[16] B. Xian, M.S. de Queiroz, D. Dawson, and I. Walker,"Task-Space Tracking Control of Robot Manipulators via Quaternion Feedback", *IEEE Transactions on Robotics and Automation*, Vol. 20, No. 1,pp.160-167, Feb. 2004.

[17] R.K. Lenz and R.Y. Tsai, "Techniques for Calibration ot the Scale Factor and Image Center for High Accuracy 3-D Machine Vision Metrology", *IEEE Trans. Pattern Analysis and Machine Intelligence,* Vol. 10, No. 5, Sept. 1988.

[18] J.J. Slotine and W. Li, A*pplied Nonlinear Control*, Englewood Cliff, NJ: Prentice Hall, 1991.